Identification of nonlinear dynamic coefficients in plain journal bearings

V. Meruane*, R. Pascual

Mechanical Engineering Department, Universidad de Chile, Beauchef 850, Santiago, Chile

Abstract

This work proposes a framework to the numerical identification of nonlinear fluid film bearing parameters from large journal orbital motion (20–60% of the bearing clearance). Nonlinear coefficients are defined by a third order Taylor expansion of bearing reaction forces and are evaluated through a least mean square in time domain technique. The journal response is obtained from a computational fluid dynamic (CFD) model of a plain journal bearing on high dynamic loading conditions. The model considers fluid–structure interaction between the fluid flow and the journal. The case in study considers a laboratory test rig. Results indicate that nonlinear coefficients have an important effect on stiffness and damping. It was found a change on nonlinear behavior occurred when the *Oil Whirl* phenomenon starts, which it is not seen in classical linear models.

Keywords: Journal bearing; Computational fluid dynamics; Transient; Identification; Large orbital motion; Nonlinear

1. Introduction

Hydrodynamic-type journal bearings are widely used in rotating machinery. This kind of bearing supports large radial loads under high-speed operating conditions. In some special conditions, they suffer from self-excited vibrations which may lead to catastrophic failures. In order to prevent such vibrations, a full understanding of the instability mechanisms is needed. Such knowledge may be used during the design stage and later during operation as a diagnosis tool.

In order to get accurate predictions of the dynamics of these bearings, it is necessary to estimate the forces produced by the fluid flow. These forces can be expressed in terms of hydrodynamic coefficients related to stiffness and damping. Linearized stiffness and damping coefficients are widely used for the stability and response analysis of rotor bearing systems.

Linearized coefficients can be predicted analytically by means of a perturbation about the equilibrium. Childs [1], Yamamoto and Ishida [2] described a methodology for the determination of linearized coefficients based on the long bearing and short bearing approximations. Rao et al. [3] determined linearized coefficients for finite length bearings based on an harmonic combination of the long and short bearings approximations (the inverse sum of the inverse of both pressures) initially proposed by Hirani et al. [4].

Numerical techniques may produce very accurate results, i.e., finite differences or finite elements methods. Linearized coefficients are predicted by means of a numerical integration of pressure gradients which are determined by a first order perturbation of the pressure distribution. Turaga et al. [5] predicted linear coefficients with a finite element method considering roughness on the surface. Rao and Sawicki [6] evaluated linear coefficients of a plain journal bearing considering cavitation effects and later (Rao and Sawicki [7]) for different types of multi-lobe bearings. Singal and Khonsari [8] presented a methodology for the determination of linearized coefficients considering the effect of inlet temperature and viscosity.

Rotors mounted on journal bearings experiment large vibrations amplitudes when traversing critical speeds. Classical numerical or analytical derivation of linearized dynamic coefficients may not be reliable for troubleshooting predictive analysis on design state. Pettinato et al. [9] studied the effect of orbit magnitude on experimentally

*Corresponding author. Tel.: +56 29 784543; fax: +56 26 896057.
E-mail addresses: vmeruane@ing.uchile.cl (V. Meruane), rpascual@ing.uchile.cl (R. Pascual).

derived bearing coefficients for a highly preloaded three-lobe journal bearing, they obtained that the coefficients remains linear for orbit sizes ranging up to 30% of the bearing clearance. San-Andrés and Santiago [10] determined experimentally the coefficients of a journal bearing under high dynamic loading conditions inducing large orbital motion (50% of bearing clearance). Their results agree favorably with analytical derived linearized coefficients.

In order to determine the validity of the linear model, it is necessary to study first the effect of nonlinearities on oil film forces. Choy et al. [11] predict nonlinear bearing stiffness coefficients of the order of odd power perturbations displacements. Linear stiffness was evaluated at the equilibrium position, while exact stiffness was obtained by a finite perturbation approach. Numerical results [12] were evaluated on different conditions in terms of the external load, rotational speed and axial misalignment. They show that for displacements far away from the equilibrium position, nonlinearities on oil film forces are significant. Sawicki and Rao [13] studied the variation of nonlinear stiffness and damping coefficients around the equilibrium position with a finite differences method. Their results indicated that oil film nonlinearities affect the journal motion at low eccentricity ratios (high Sommerfeld number) with a wide variation on the stiffness and damping coefficients.

In this work the linear and nonlinear stiffness and damping coefficients are estimated from medium to large journal orbit (whirl orbit ratio from 20% to 60% of the bearing clearance) on operating conditions, by means of a least mean square in time domain technique originally proposed by Zhou et al. [14]. It considers a 3D plain journal bearing under transient conditions with fluid–structure interaction between the lubricant and the journal. Solving the fully coupled solution of fluid flows with structural interactions give us a powerful tool that allows to directly obtain the nonlinear transient response under different operation conditions.

The remainder of this work is organized as follows. Section 2 presents general antecedents and related research on journal bearing coefficients. Section 3 presents the nonlinear model proposed and the parameter identification method used. Section 4 shows a general outline of the numerical identification method proposed. Section 5 presents the case in study, defining the journal bearing properties and dimensions. Section 5.1 provides numerical issues, assumptions and properties used in the computational fluid dynamics (CFD) simulation. Section 5.2 shows the numerical results obtained in the CFD simulation in terms of both the nonlinear transient journal orbit and pressure distribution for different journal eccentricities. The numerical results are compared with analytical expressions for pressure distribution with the long, the short and the harmonic combination bearing approximations. The predicted linear stiffness and damping coefficients are compared with linearized analytical expressions derived from the short and long bearing approximations. Nonlinear damping and stiffness coefficients are determined and the effects of nonlinearities in the journal response are studied. Finally, the conclusions and forthcoming work are presented.

2. Theoretical background

This section contains the theoretical background necessary for the validation of the numerical results. In order to be self-contained we explain some concepts already formulated in literature.

The Reynolds differential equation for a dynamically loaded journal bearing with the assumptions of isoviscous, Newtonian, incompressible and laminar flow is given as

$$\frac{1}{R^2}\frac{\partial}{\partial\theta}\left(\frac{h^3}{\mu}\frac{\partial p}{\partial\theta}\right)+\frac{\partial}{\partial z}\left(\frac{h^3}{\mu}\frac{\partial p}{\partial z}\right)=\frac{6U}{R}\frac{\partial h}{\partial\theta}+12\frac{\partial h}{\partial t}, \tag{1}$$

where R is the journal radius, θ is the circumferential coordinate in a fixed frame, h is the film thickness, z is the axial coordinate, μ is the fluid dynamic viscosity, and U is the journal tangential velocity.

Pinkus and Sternlicht [15] presented some analytical solutions to Eq. (1), but an analytical solution of Eq. (1) for arbitrary geometry cylindrical bearings is in general not feasible. Most frequently, numerical methods are employed to solve the Reynolds equation and to obtain the performance characteristics of bearing configurations of particular interest.

Eq. (1) can also be solved using the assumption of 1-D bearing, i.e., infinitely long or infinitely short bearing approximations. Hori [19] [1959] simplified the equation assuming that the length of the bearing is infinitely long (the *long bearing approximation*). Funakawa and Tatara [20] [1964] explained experimental results more accurately assuming that the bearing is infinitely short (the *short bearing approximation*). The short bearing approximation gives accurate results for ratios of the bearing length and diameter under 0.5 (L/D on Fig. 1) and for small to moderate values of the journal eccentricity (eccentricity ratios $e/c<0.7$). The long bearing approximation gives accurate results for values of (L/D) higher than 2. Industrial bearings usually have a ratio L/D in the range (0.5, 1), for such values, Eq. (1) is solved numerically.

In the short bearing approximation, it is considered that the pressure gradient in the z direction (Fig. 1) is considerably larger than that in the θ direction ($\partial p/\partial\theta \ll \partial p/\partial z$). The pressure distribution can be obtained by direct integration of the Reynolds equation after ignoring the term representing the pressure variation in the θ direction:

$$P_s(\varphi,z)=\frac{3\mu}{c^2(1+\kappa\cos\varphi)^3}\times(2\dot{\kappa}\cos\varphi-\kappa(\omega+2\dot{\theta})\sin\varphi)\left(z^2-\frac{L^2}{4}\right), \tag{2}$$

where κ is the journal eccentricity ratio (e/c) and φ is the circumferential coordinate in a rotating frame (Fig. 1). The

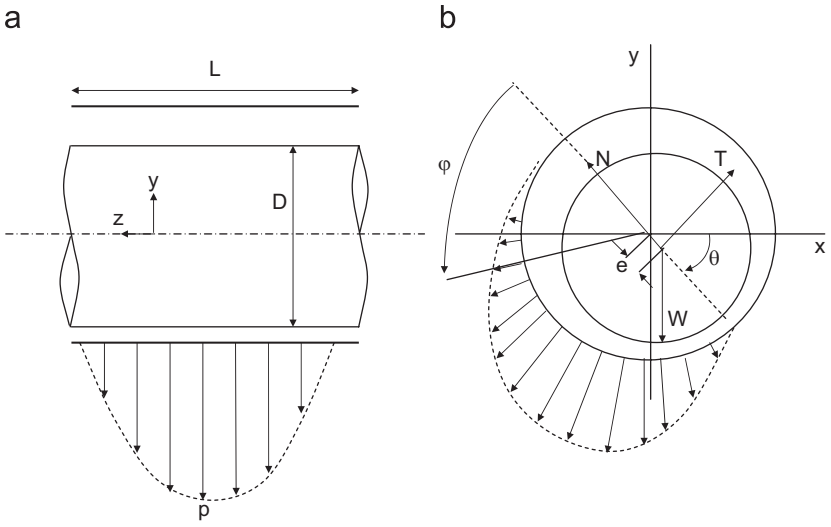

Fig. 1. Oil film forces and journal loci: (a) pressure distribution; (b) pressure distribution and oil film force.

long bearing approximation assumes that the pressure does not change in the z direction (i.e., $\partial p/\partial z = 0$):

$$P_{\mathrm{l}}(\varphi) = \frac{-6\mu r^2}{c^2(1+\kappa\cos\varphi)^2}\left(\dot{\kappa}\cos\varphi - \frac{\kappa}{(2+\kappa^2)}(\omega - 2\dot{\theta})\sin\varphi\right) \times(2+\kappa\cos\varphi). \tag{3}$$

As previously mentioned, for L/D in the range (0.5, 1) both the short and long bearing approximations are inadequate. Hirani et al. [4] defined an expression for the pressure distribution in a finite length bearing by combining harmonically the short and long bearing solutions in the form:

$$\frac{1}{P} = \frac{1}{P_{\mathrm{s}}} + \frac{1}{P_{\mathrm{l}}}. \tag{4}$$

From the given expressions for the pressure distribution we know that when the journal is rotating in the equilibrium position ($\dot{\kappa} = \dot{\varphi} = 0$), the peripheral pressure distribution in the z plane is symmetrical about the point $\varphi = 0$ to π and is negative in the zone from $\varphi = \pi$ to 2π in Fig. 1. This pressure distribution is called *Sommerfeld condition* and holds when the pressure magnitude is very small. However, in practical journal bearings in the zone from $\varphi = \pi$ to 2π may occur evaporation of the lubricant and axial airflow from both ends, this leads to the pressure in this zone to be almost zero (i.e., the atmospheric pressure) instead of negative. Taking this situation into consideration, the pressure in the zone from $\varphi = \pi$ to 2π is set as $p = 0$, which is known as the *Gumbel condition*.

The fluid film forces (Fig. 1) are given by

$$N = -R\int_{-l/2}^{l/2}\int_0^{\alpha} p\cos\varphi\,\mathrm{d}\varphi\,\mathrm{d}z,$$
$$T = -R\int_{-l/2}^{l/2}\int_0^{\alpha} p\sin\varphi\,\mathrm{d}\varphi\,\mathrm{d}z, \tag{5}$$

where $\alpha = \pi$ for the Gumbel condition (π-film) and 2π for the Sommerfeld condition. These expressions for the fluid film forces are valid only in the equilibrium position. Under dynamic conditions the film length would vary.

The Sommerfeld short bearing approximation results in the following expressions for the oil film forces:

$$N = \frac{1}{2}\mu\left(\frac{r}{c}\right)^2\frac{l^3}{r}\left[\frac{2\pi\dot{\kappa}(1+2\kappa^2)}{(1-\kappa^2)^{5/2}}\right], \tag{6}$$

$$T = \frac{1}{2}\mu\left(\frac{r}{c}\right)^2\frac{l^3}{r}\left[\frac{\pi\kappa(w+2\dot{\theta})}{(1-\kappa^2)^{3/2}}\right] \tag{7}$$

and for the Sommerfeld long bearing approximation,

$$N = 6\mu\left(\frac{r}{c}\right)^2 rl\left[\frac{4\dot{\kappa}}{(1-\kappa^2)^{3/2}}\left\{\frac{\pi}{2} - \frac{8}{\pi(2+\kappa^2)}\right\}\right], \tag{8}$$

$$T = 6\mu\left(\frac{r}{c}\right)^2 rl\left[\frac{2\pi\kappa(w-2\dot{\theta})}{(2+\kappa^2)(1-\kappa^2)^{1/2}}\right]. \tag{9}$$

The equilibrium position of the journal center is determined by the balance between the gravity load W and the oil film forces (F_0, N_0). The equilibrium position is given by the bearing geometry and by the *Sommerfeld* number $S = (\frac{r}{c})^2\mu n/p_m$, where n(rps) is the rotational speed and $p_m = F_0/2rl$ is the average bearing pressure. To determine the bearing dynamic coefficients, the expression for the equilibrium forces are derived when the rotor deviates slightly from the equilibrium and then are linearized.

3. Numerical identification method

Stiffness and damping coefficients are obtained from a Taylor series expansion of the bearing fluid film forces in terms of both perturbation displacements and velocities. Nonlinearities in bearing forces are obtained by including high order displacements and velocity perturbations on oil film formula. choy et al. [11] included coefficients of odd power (3rd, 5th, 7th) for displacements. Sawicki and Rao [13] included the first and second order terms for

displacements and velocities, they also considered the cross combination terms (i.e., $\Delta x \Delta y$). In this work we considered until third order terms on the Taylor expansion. The oil film force increment (dynamic oil film force) is a function of the displacements (x, y) and velocities $(\dot{x}, \dot{y})$ to the static position (x_0, y_0), which can be represented as follows:

$$\begin{bmatrix} \Delta f_x \\ \Delta f_y \end{bmatrix} = \begin{bmatrix} k_{xx} & k_{xy} \\ k_{yx} & k_{yy} \end{bmatrix} \begin{bmatrix} \Delta x \\ \Delta y \end{bmatrix} + \begin{bmatrix} c_{xx} & c_{xy} \\ c_{yx} & c_{yy} \end{bmatrix} \begin{bmatrix} \Delta \dot{x} \\ \Delta \dot{y} \end{bmatrix}, \tag{10}$$

where k_{ij} are the bearing stiffness coefficients, c_{ij} are the bearing damping coefficients, and Δf_i is the recognized oil film forced increment. The damping and stiffness coefficients can be represented as follows:

$$k_{ij} = k_{ij_0} + k_{ijx}\Delta x + k_{ijy}\Delta y + k_{ijxx}\Delta x^2 + k_{ijxy}\Delta x \Delta y + k_{ijyy}\Delta y^2, \tag{11}$$

$$c_{ij} = c_{ij_0} + c_{ijx}\Delta \dot{x} + c_{ijy}\Delta \dot{y} + c_{ijxx}\Delta \dot{x}^2 + c_{ijxy}\Delta \dot{x}\Delta \dot{y} + c_{ijyy}\Delta \dot{y}^2, \tag{12}$$

where k_{ij_0}, c_{ij_0} are the linear stiffness and damping coefficients. k_{ijk}, c_{ijk} are the second order nonlinear stiffness and damping coefficients, and k_{ijkm}, c_{ijkm} are the third order nonlinear stiffness and damping coefficients. Non-dimensional values of these coefficients can be represented as follows:

$$K_{ij} = \frac{ck_{ij}}{F_0}, \quad K_{ijk} = \frac{c^2 k_{ijk}}{F_0}, \quad K_{ijkm} = \frac{c^3 k_{ijkm}}{F_0}, \tag{13}$$

$$C_{ij} = \frac{c\omega c_{ij}}{F_0}, \quad C_{ijk} = \frac{c^2\omega^2 c_{ijk}}{F_0}, \quad C_{ijkm} = \frac{c^3\omega^3 c_{ijkm}}{F_0}. \tag{14}$$

The coefficients are estimated from the journal response to an external excitation load. If the external forces acting on the bearing are known, the oil film forces (f_x, f_y) can be calculated as

$$f_x = F_x(t) - m\Delta \ddot{x}, \quad f_y = F_y(t) - m\Delta \ddot{y}, \tag{15}$$

where F_x, F_x are external excitation forces, and $\ddot{x}$, $\ddot{y}$ are the journal accelerations in the x and y directions. The bearing dynamic parameters can be determined then by minimizing the difference between f_x and Δf_x. The correlation is made by means of a least mean square method, the error function is defined as [14]:

$$\varepsilon_k = f_x(k) - \Delta f_x(k). \tag{16}$$

The sum of the square of the errors is given by $E = \sum_{n=1}^{4}\sum_{k=1}^{P}(\varepsilon_k)^2$. The coefficients are then estimated by minimizing this error function.

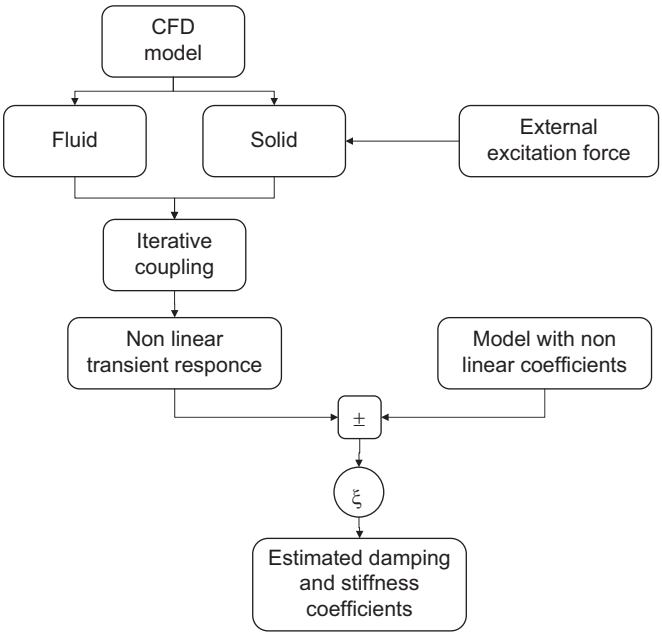

Fig. 2. Proposed scheme.

4. Proposed scheme

In Fig. 2 is outlined the proposed scheme for the numerical identification method. The numerical model is developed on the CFD software ADINA 8.1, and it is defined by a fluid and a solid model. The solid model represents the journal/shaft that is excited by two independent sinusoidal forces. The fluid model represents the oil film. The bearing as modelled has a plain journal bearing.

The journal bearing properties were obtained from a real test rig described in Section 5. Numerical assumptions, boundary conditions and the numerical method used are described in Section 5.1. Both the solid and fluid models are fully coupled and solve iteratively in order to obtain the nonlinear transient response of the bearing.

The magnitude of the excitation force is defined as half of the bearing load (journal and shaft weight), in this way assuring a large journal orbital motion.

Finally, the linear and nonlinear dynamic parameters are obtained from the nonlinear journal response as described in Section 3, by fitting a model with concentrated parameters based on a third order Taylor expansion of the oil film formula.

5. Case study

The bearing properties were obtained from a plain journal bearing which is part of the Rotor Kit Bently Nevada 2000 [16] available (Fig. 3).

This rotor contains an oil pump that feeds the journal bearing with an inlet pressure up to 120 kPa. This pump is connected to the oil bearing assembly which contains the

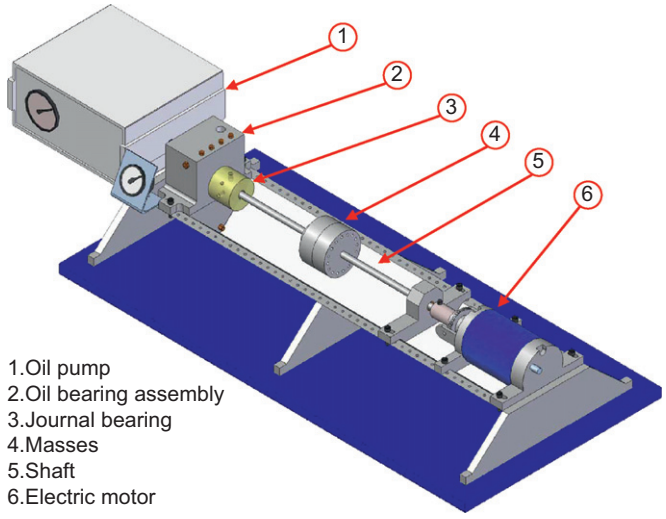

Fig. 3. Laboratory test rig.

Table 1
Journal bearing properties

Symbol	Description	Value	Unit
c	Radial clearance	6.5	*mils*
D	Journal diameter	1	in
L	Bearing length	1	in
W	Journal load	9.6	N
ρ	Lubricant density	870	kg/m^3
μ	Lubricant viscosity	2.5×10^{-2}	$kg/m\,s$

bearing supporting structure and the oil recipient. Shaft rotational speed varies between 500 and 8000 rpm. The journal bearing properties are listed in Table 1.

5.1. CFD simulation

Although the scope of CFD applications include heat transfer, variable fluid properties, no Newtonian fluids and turbulent model, this work focuses on determining the dynamic bearing coefficients. The model considers constant fluid properties, no slip on the boundaries, incompressible and laminar flow.

In a realistic model it would be necessary to implement a thermohydrodynamic analysis of the bearing. Since the lubricant viscosity strongly depends on temperature and the assumptions of constant viscosity or effective viscosity become untenable.

The model does not consider cavitation, so is expected to obtain a solution similar to the analytical one with the Sommerfeld condition ($2\pi film$).

The fluid external wall is fixed and the moving (interior) wall interacts with the solid and has a tangential velocity equal to the rotational speed. Side walls have zero pressure.

The external wall of the solid model has a fluid–solid interaction condition. The solid model is modelled with body load gravity and the hypothesis of large displacements and small strains kinematics which implies a total Lagrangian formulation.

Table 2
Mesh-density sensitivity analysis

$(r,z)=(5,10)$			$(\theta,r)=(100,3)$			$(\theta,z)=(100,20)$		
θ	Pmax (Pa)	Dif. (%)	z	Pmax (Pa)	Dif. (%)	r	Pmax (Pa)	Dif. (%)
60	19 438	5.031	10	18 262	1.191	3	18 262	5.496
80	18 608	0.546	20	18 092	0.249	4	18 426	4.647
100	18 492	0.081	30	18 046	0.006	5	19 170	0.797
120	18 507	–	40	18 047	–	6	19 324	–

Maximum pressure vs number of divisions (r,θ,z).

A transient simulation was performed in *ADINA 8.1* 2003 [17]. Time integration is handled through a second order trapezoidal method (TR-BDF Trapezoidal Rule Backward Differentiation Formula). The iteration method used is the Newton–Raphson method, with a direct solver based on the Gauss elimination method (solver *sparse* of ADINA) which preserves the matrix sparsity, thus reducing dramatically the storage and computer time. The interaction between the fluid film and the solid parts of the bearing is solved by using an iterative method. In this solution, the fluid and solid equations are solved individually and sequentially, using the latest information provided from another part of the coupled system considering displacements and stress relaxation factors. This iteration is continued until convergence is reached. Convergence speed was accelerated by using relaxation factors of 0.5 for displacements and stress.

Mesh aspect ratio influences the quality of the results and it is usually chosen in a value below 2. Such rule is difficult to follow in this application due to the magnitude difference between the thickness of the fluid and the dimensions of the bearing. It would need extremely large number of mesh elements. Previous works show that it is possible to handle greater mesh aspect ratio in the journal bearing case, Keogh et al. [18] used a mesh aspect ratio of 500, because flows change very slowly in circumferential and axial directions. Mesh density was selected after a sensitivity analysis on the maximum pressure as a function of the number of divisions in the circumferential (θ), radial (r) and axial (z) directions with the journal fixed in the center position. Results are given in Table 2 with respect to the situation with highest density mesh.

The solution is more sensitive to the circumferential and radial mesh density. The final fluid model was defined with $5 \times 120 \times 10$ (r,θ,z) divisions (mesh aspect ratio of 77), with a total of 36 000 3D fluid elements. The solid model was defined with $3 \times 120 \times 2$ (r,θ,z) divisions, with a total of 480 3D solid elements.

Total integration time was defined until a permanent oscillation orbit was reached. Fig. 4 shows that for a nondimensional time ($\tau = \omega t$) of 400 this condition is reached. In each simulation 1000 time steps were performed with a nondimensional time step of $\Delta\tau = 0.4$.

5.2. Numerical results

Fig. 5 shows the free response of the journal obtained at different rotational speeds with the CFD model. The rotor shows sub-harmonic vibrations as it is shown in Fig. 6. The dominant frequency is 0.48× which corresponds to the well-known *Oil Whirl* phenomenon (expected between 0.38× to 0.49×, depending on the system). It can be seen that for the velocities 1000 and 2000 rpm *Oil Whirl* appear only at the beginning on transient stage, and from

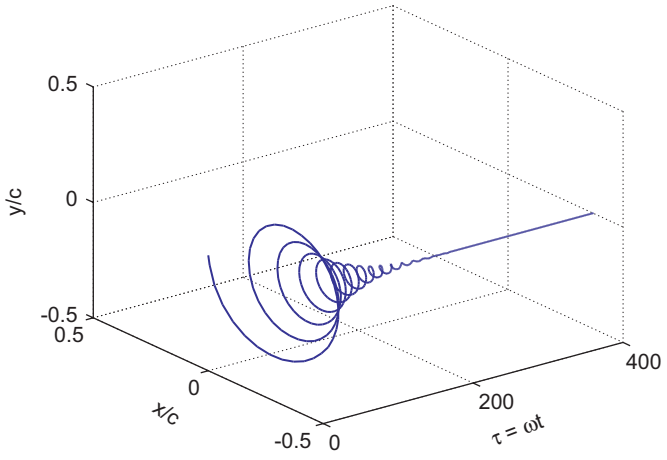

Fig. 4. Journal oscillation orbit at 1000 rpm.

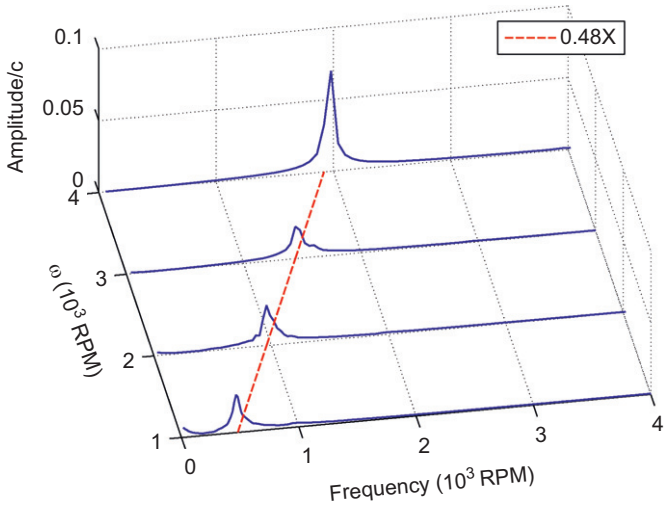

Fig. 6. Spectrum of journal orbit.

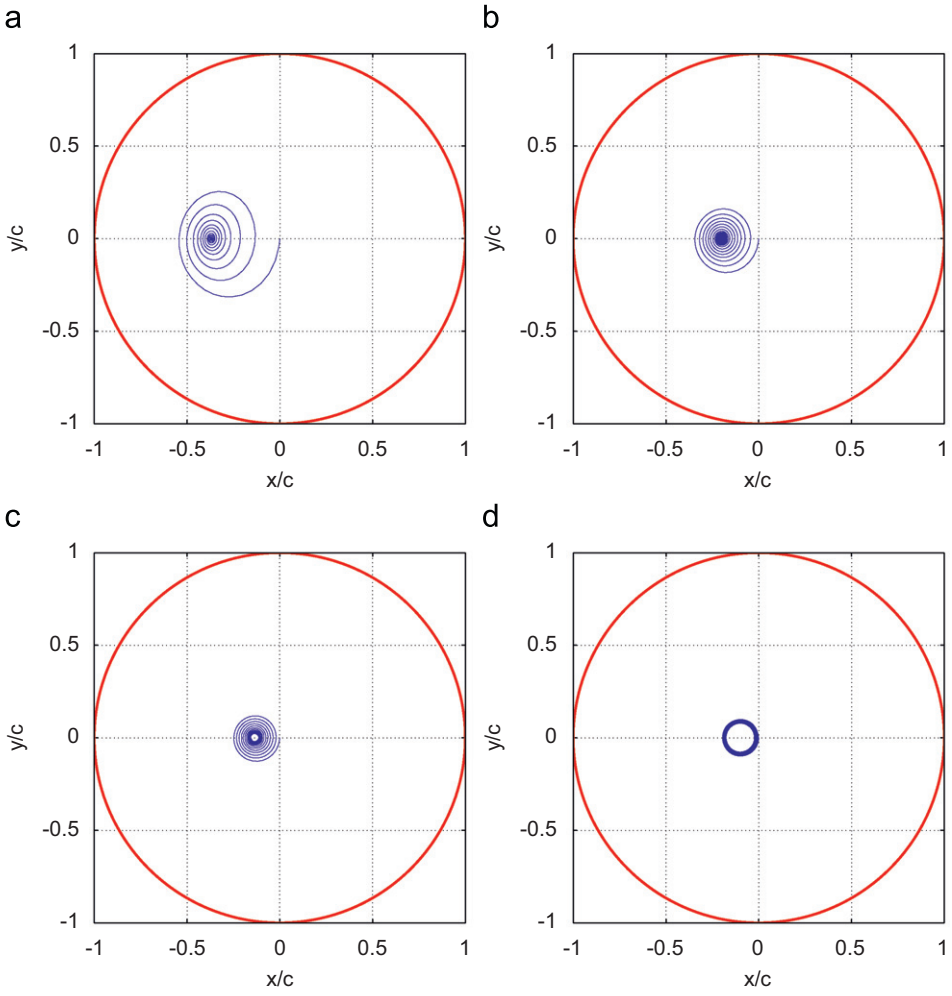

Fig. 5. Journal whirl orbit: (a) 1000 rpm; (b) 2000 rpm; (c) 3000 rpm; (d) 4000 rpm.

3000 rpm starts the *Oil Whirl* phenomenon. This is consistent with the experimental experience that shows that there is a velocity from which the *Oil Whirl* starts. Let us recall that this is a self-excited vibration since no dynamic external forces act on the system.

Fig. 7(a) shows the pressure distribution obtained numerically with a rotational speed of 1000 rpm, at this velocity the equilibrium position has an eccentricity ratio of $\kappa_0 = 0.37$. The pressure distribution is compared to the expressions for short bearing, long bearing and their harmonic combination (Fig. 7). The numerical solution is very similar to the one obtained with the harmonic combination.

A sensitivity analysis was performed for others eccentricity ratios as it is shown in Fig. 8, where the average pressure is plotted in the z direction for three different eccentricity ratios.

Fig. 8 shows that for this bearing configuration, i.e., $L/D = 1$, the harmonic combination gives the best approximation near the equilibrium position and for large eccentricity ratios. From this, it can also be seen that the short bearing and long bearing approximation are valid only for small eccentricity ratios, for large eccentricity ratios these approximations give pressure values to high.

In the identification parameter procedure the journal was excited by two independent sinusoidal forces in the

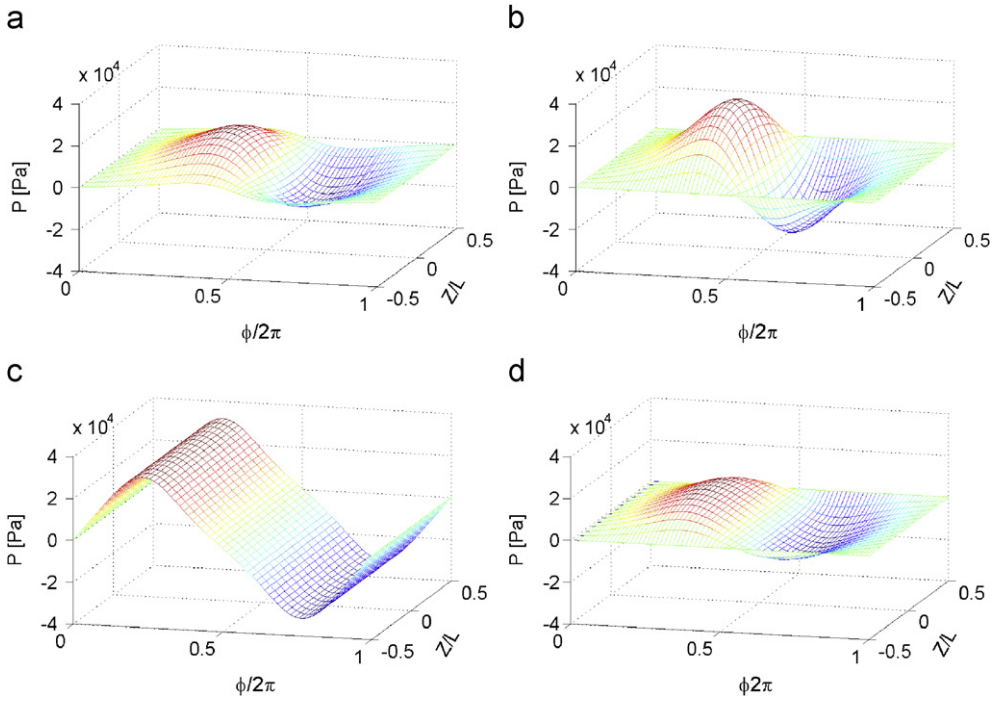

Fig. 7. Pressure distribution using different models at 1000 rpm and $\kappa = 0.37$. (a) Numerical; (b) short bearing; (c) long bearing; (d) harmonic combination.

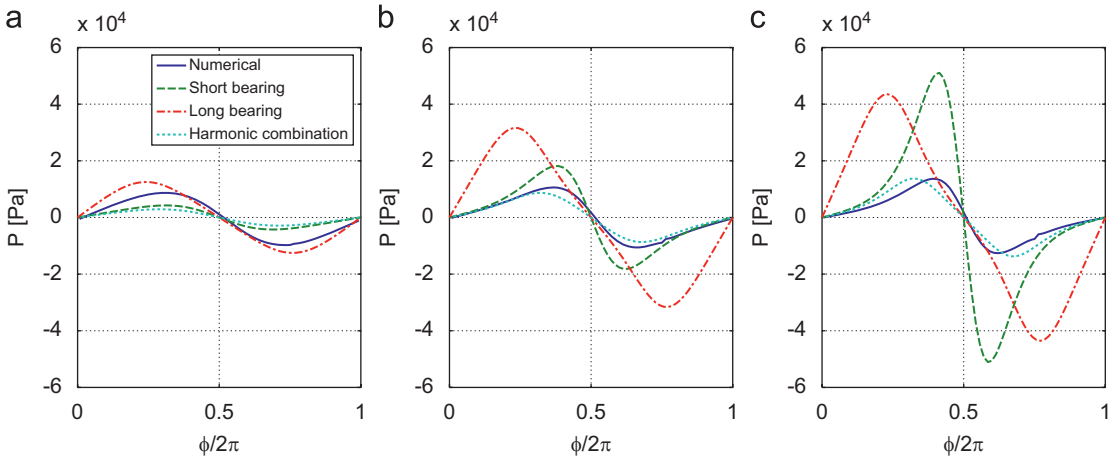

Fig. 8. Average pressure distribution in the z direction, at 1000 rpm for three different eccentricities. (a) $\kappa = 0.13$; (b) $\kappa = 0.37$; (c) $\kappa = 0.54$.

horizontal x and vertical y directions. The magnitude of the excitation force was defined as half of the bearing load (journal and shaft weight). Fig. 9 shows forced response before (2000 rpm) and after (2500 rpm) the *Oil Whirl* phenomenon.

Journal coefficients were determined by minimizing the quadratic error function between f and Δf as was defined in Section 3. The optimization method used is the generalized reduced gradient, GRG2, presented by Lasdon and Waren (1979 [21], 1984 [22]) which solves an optimization problem with a nonlinear objective function and nonlinear constraints. Fig. 10 shows the resultant fitting of Δf_x and Δf_y when a model with only linear coefficients is used and considering the nonlinear terms. Fig. 11 shows the same as Fig. 10 but after *Oil Whirl*.

The results show a much better fit with the nonlinear model. It is also possible to see that the *Oil Whirl* phenomenon does not affect the fitting and therefore neither the parameter identification procedure.

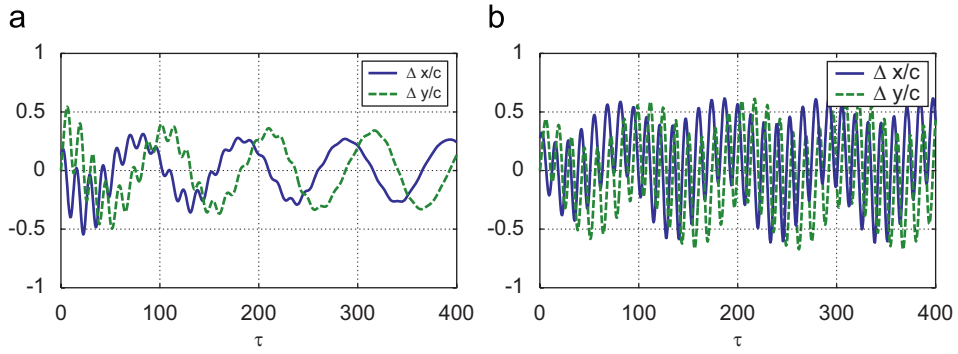

Fig. 9. Forced response before and after the *Oil Whirl* phenomenon. (a) 2000 rpm. (b) 2500 rpm.

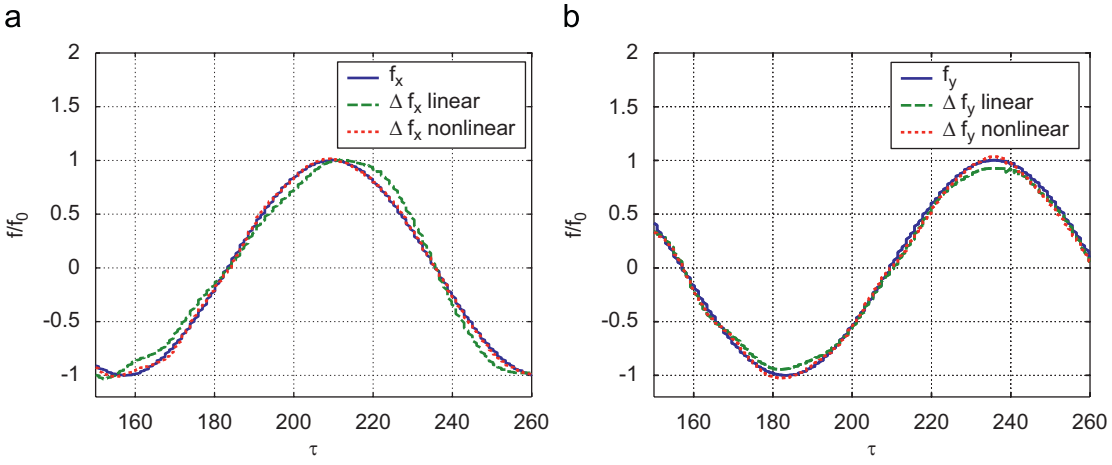

Fig. 10. Fitting of (a) Δf_x and (b) Δf_y for a rotational speed of 2000 rpm (before *Oil Whirl*).

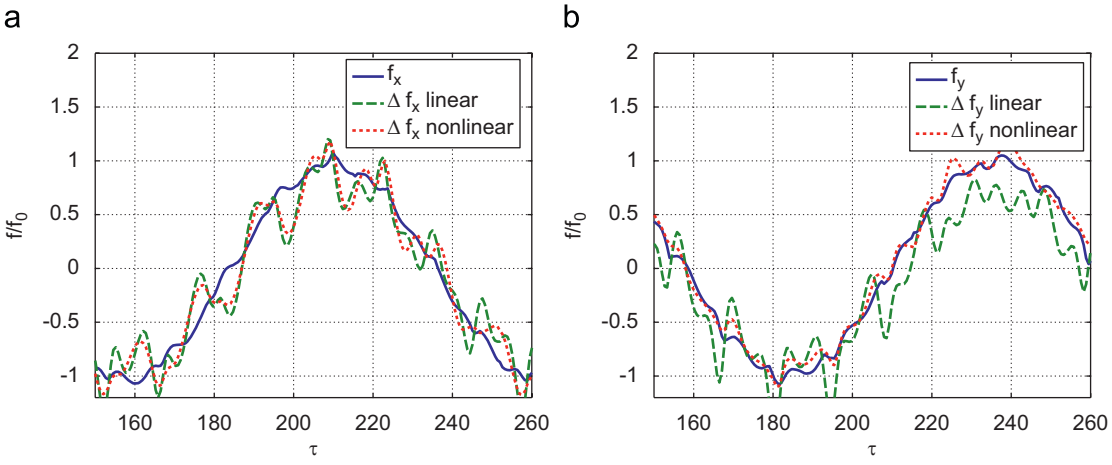

Fig. 11. Fitting of (a) Δf_x and (b) Δf_y for a rotational speed of 2500 rpm (after *Oil Whirl*).

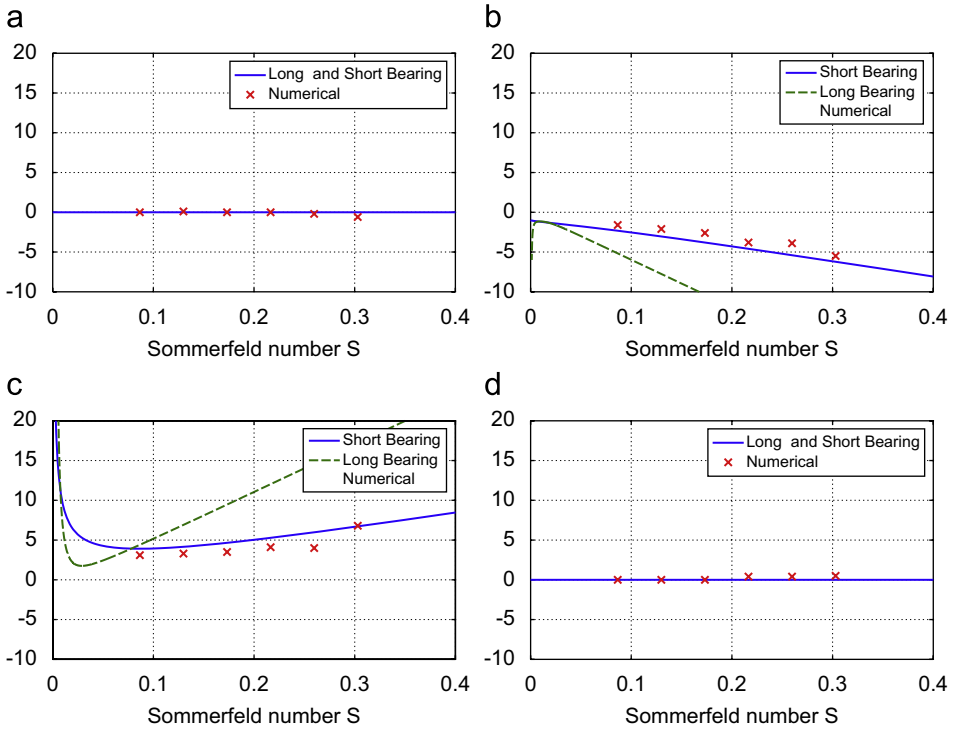

Fig. 12. Nondimensional linear stiffness coefficients. (a) K_{xx_0}; (b) K_{xy_0}; (c) K_{yx_0}; (d) K_{yy_0}.

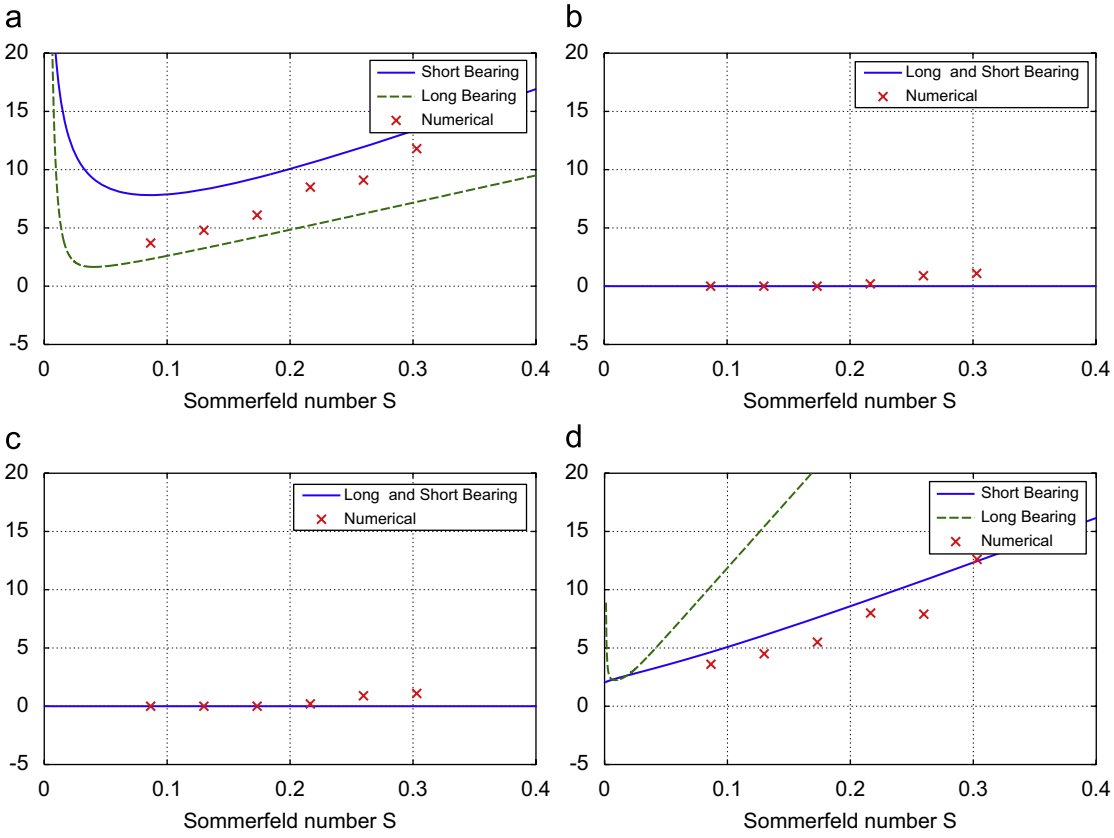

Fig. 13. Nondimensional linear damping coefficients. (a) C_{xx_0}; (b) C_{xy_0}; (c) C_{yx_0}; (d) C_{yy_0}.

Figs. 12 and 13 show the linear stiffness and damping coefficients obtained with the proposed numerical method. The coefficients are compared to the analytical values expected for the short and long bearing approximations.

Linear stiffness coefficients are surprisingly close to the analytically linearized coefficients for the short bearing approximation. On the other hand, linear damping coefficients are between the long and the short bearing approximations for C_{xx} and they are closer to the short bearing approximation for C_{yy}.

Nonlinear stiffness coefficients obtained are shown in Fig. 14. A change in the coefficients values can be observed when the *Oil Whirl* phenomenon starts ($S = 0.21$), this shows a change in the bearing behavior when this phenomenon occurs.

To study the effect of nonlinear terms in the effective stiffness, the coefficients were evaluated from Eq. (9) for the orbital motions obtained on simulations. Fig. 15 shows the absolute variation on nondimensional stiffness coefficients along the journal orbit before and after *Oil Whirl*.

It is observed from Fig. 15 that before *Oil Whirl* occurs (1000 rpm) the absolute variation on nondimensional stiffness coefficients because of nonlinearities is about 0.2. When *Oil Whirl* starts (3500 rpm) this variation is increased into a value of 0.7 approximately. In both the cases oil film nonlinearities have an important effect on the effective stiffness and must be considered.

Fig. 16 shows the nonlinear damping coefficients obtained. If the absolute variation of the nondimensional damping coefficients along the journal orbit is analyzed

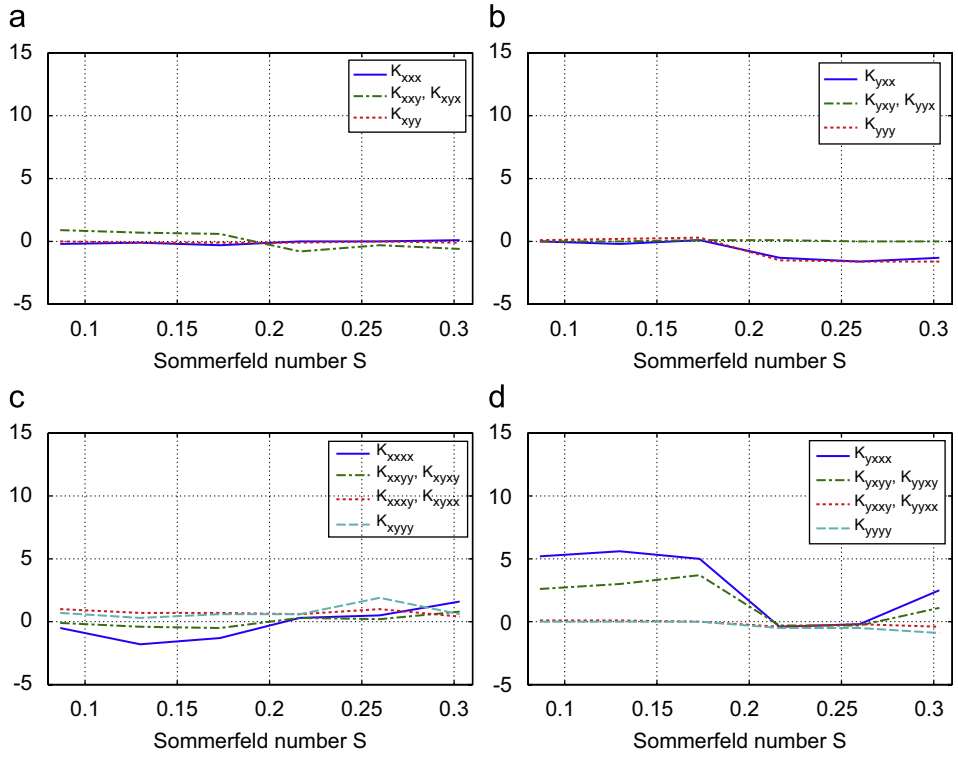

Fig. 14. Nondimensional nonlinear stiffness coefficients.

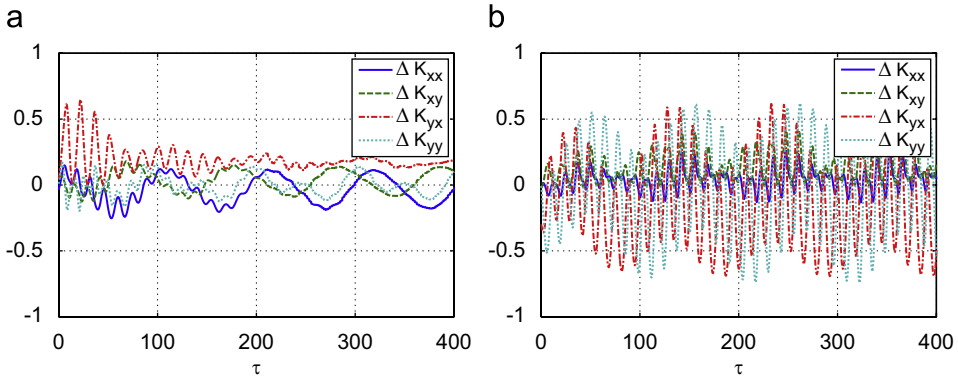

Fig. 15. Absolute variation on nondimensional stiffness coefficients before and after the *Oil Whirl* phenomenon. (a) 2000 rpm; (b) 2500 rpm.

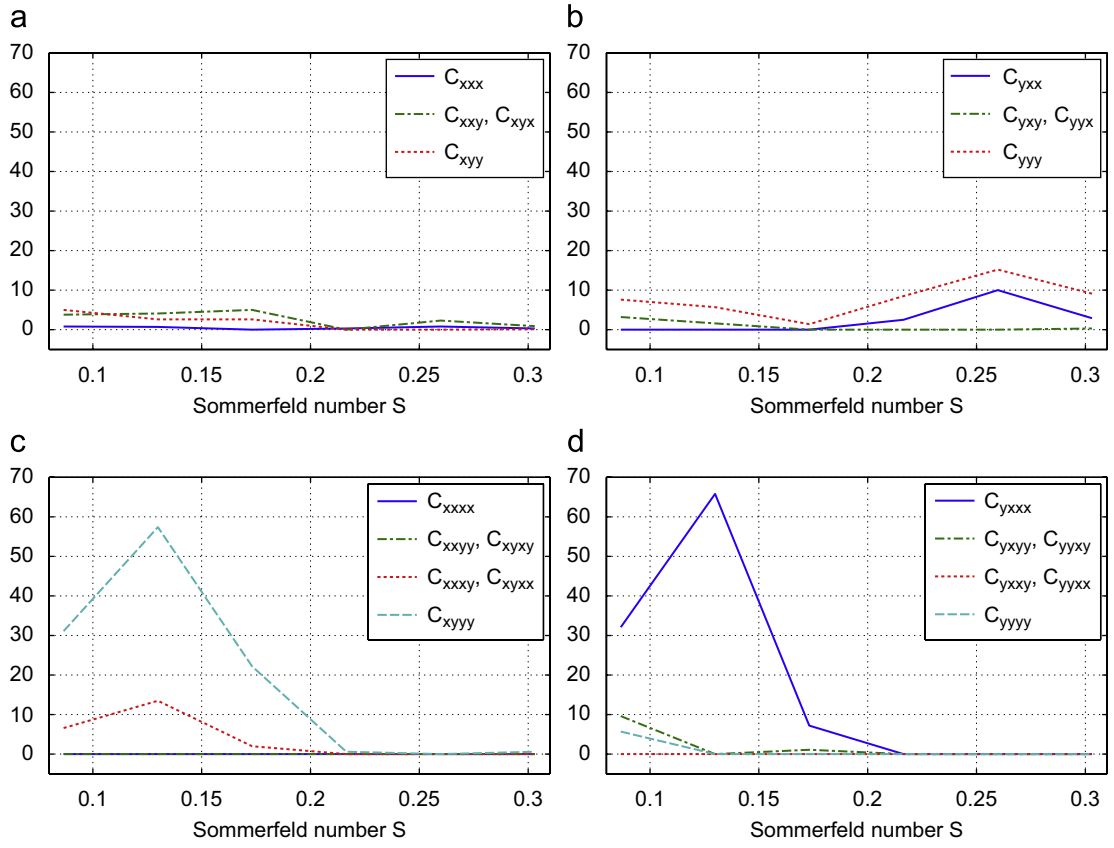

Fig. 16. Nondimensional nonlinear damping coefficients.

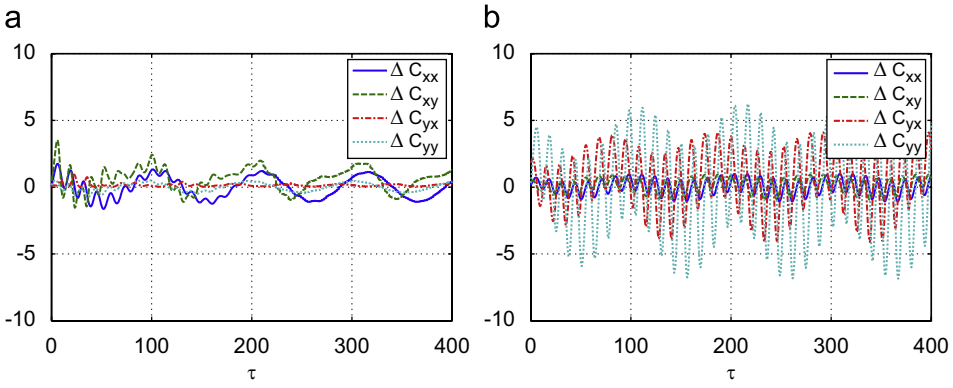

Fig. 17. Absolute variation on nondimensional damping coefficients before and after the *Oil Whirl* phenomenon. (a) 2000 rpm; (b) 2500 rpm.

(Fig. 17), it is obtained that before the *Oil Whirl* this variation gets to a value of 2 and during the *Oil Whirl* phenomenon has an important increase getting to a variation up to 7. The absolute variation on damping coefficients is in the same order of magnitude that the coefficients, obtaining a variation of about 90% for C_{yy}. This shows the importance of nonlinearities on the damping coefficients.

6. Closure

The present work introduces a general framework to identify linear and nonlinear stiffness and damping coefficients on journal bearings. Coefficients were estimated in typical operation conditions, this implies large journal orbital motion and even during the *Oil Whirl* phenomenon. The framework proposed here has the advantage to determine accurately the nonlinear transient response for different operational conditions. It is able to identify dynamic parameters and it allows to make stability analysis on design state saving all the experimental effort. The formulation improves results since it considers large journal orbit due to high dynamic loading which is usual on real industrial cases where this type of bearing is used.

The results of the case in the study show that linearized analytical coefficients agree reasonably with linear coefficients estimated numerically considering a nonlinear model. Nonlinear coefficients were found to have an important effect on effective stiffness and damping.

It was found that the *Oil Whirl* phenomenon causes a change on the nonlinear behavior of the bearing (changing nonlinear coefficients), which it is not seen when using linear models. Considering this, it is important in a stability analysis to consider the nonlinear terms and their change when *Oil Whirl* phenomenon starts.

The parameter identification method defined shows to be an efficient and fast algorithm to determine the stiffness and damping coefficients from the journal forced response with large journal orbit motion, considering linear and nonlinear terms in the Taylor expansion.

The present model represents a powerful tool to predict accurately non linear transient phenomena like response to starts, stops and *Oil Whirl/Whip* phenomena. Although the simulated model was very simple (no cavitation, constant fluid properties, etc.), the extension to handle more realistic cases is straightforward. Further works consider developing a 3D CFD model taking into account cavitation, temperature distribution and the external oil inlet pressure. The study of instabilities is also important when a nonlinear model is considered.

Acknowledgments

The authors wish to acknowledge the partial financial support of this study by the Fondo Nacional de Desarrollo Científico Y Tecnológico (FONDECYT) of the Chilean government, project 1030943.

References

[1] Childs D. Turbomachinery rotordynamics phenomena, modeling, and analysis. New York: Wiley; 1993.
[2] Yamamoto T, Ishida Y. Linear and nonlinear rotordynamics a modern treatment with applications. New York: Wiley; 2001.
[3] Rao TVVLN, Biswas S, Athre K. A methodology for dynamic coefficients and nonlinear response of multi-lobe journal bearings. Tribol Trans 2001;44(1):111–7.
[4] Hirani H, Athre K, Biswas S. Rapid and globally convergent method for dynamically loaded journal bearing design. Proc Inst Mech Eng Part J 1998;212:207–14.
[5] Turaga R, Sekhar AS, Majumdar BC. Stability analysis of a rigid rotor supported on hydrodynamic journal bearings with rough surfaces using the stochastic finite element method. Proc Inst Mech Eng Part J 1998;212:121–30.
[6] Rao TVVLN, Sawicki JT. Linear stability analysis for a hydrodynamic journal bearing considering cavitation effects. Tribol Trans 2002;45(4):450–6.
[7] Rao TVVLN, Sawicki JT. Dynamic coefficient prediction in multilobe journal bearings using a mass conservation algorithm. Tribol Trans 2003;46(3):414–20.
[8] Singal S, Khonsari MM. A simplified thermohydrodynamic stability analysis of journal bearings. Proc Inst Mech Eng Part J 2005;219: 225–34.
[9] Pettinato B, Flack RD, Barrett LE. Test results for a highly preloaded three-lobe journal bearing—effect of load orientation on static and dynamic characteristics. J Soc Tribol Lubr Eng 2001: 23–30.
[10] San-Andrés L, Santiago OD. Identification of journal bearing force coefficcients under high dynamic loading centered static operation. Tribol Trans 2005;48:9–17.
[11] Choy FK, Braun MJ, Hu Y. Nonlinear effects in a plain journal bearing: part 1—analytical study. ASME J Tribol 1991;113: 555–62.
[12] Choy FK, Braun MJ, Hu Y. Nonlinear effects in a plain journal bearing: part 2—results. ASME J Tribol 1991;113:563–70.
[13] Sawicki JT, Rao TVVLN. A nonlinear model for prediction of dynamic coefficients in a hydrodynamic journal bearing. Int J Rotating Mach 2004;10(6):507–13.
[14] Zhou H, Zhao S, Xu H, Zhu J. An experimental study on oil-film dynamic coefficients. Tribol Int 2004;37:245–53.
[15] Pinkus O, Sternlicht B. Theory of hydrodynamic lubrication. New York: McGraw-Hill; 1961.
[16] Nevada B. Rotor kit servofluid control bearing option manual. Nevada: Bently; 2000.
[17] ADINA. ADINA 8.1 user guide. ADINA R & D Inc; 2003.
[18] Keogh PS, Gomiciaga R, Khonsari MM. Cfd based design techniques for termal prediction in a generic two-axial groove hydrodynamic journal bearing. J Tribol 1997;119:428–36.
[19] Hori Y. A theory of oil whip. J Appl Mech 1959;26(2):189–98.
[20] Funakawa M, Tatara A. Stability criterion of an elastic rotor in journal bearings. Trans JSME 1964;30(218):1238–44.
[21] Lasdon LS, Waren AD. Generalized reduced gradient software for linearly and nonlinearly constrained problems in design and implementation of optimization software. Sijthoff and Noordhof: H.J. Greenberg; 1979.
[22] Lasdon LS, Waren AD. GRG2 User's guide. School of Business Administration, University of Texas at Austin, 1984.